

# Collective and Single-Molecule Interactions of $\alpha_5\beta_1$ Integrins

Efrosini Kokkoli,<sup>†</sup> Sarah E. Ochsenhirt,<sup>†</sup> and Matthew Tirrell<sup>\*‡</sup>

Department of Chemical Engineering and Materials Science, University of Minnesota, Minneapolis, Minnesota 55455 and Department of Chemical Engineering, University of California, Santa Barbara, California 93106

Received August 27, 2003. In Final Form: December 28, 2003

A novel biomimetic system was used to study collective and single-molecule interactions of the  $\alpha_5\beta_1$  receptor-GRGDSP ligand system with an atomic force microscope (AFM). Bioartificial membranes, which display peptides that mimic the cell adhesion domain of the extracellular matrix protein fibronectin, are constructed from peptide-amphiphiles. The interaction measured with the immobilized  $\alpha_5\beta_1$  integrins and GRGDSP peptide-amphiphiles is specifically related to the integrin-peptide binding. It is affected by divalent cations in a way that accurately mimics the adhesion function of the  $\alpha_5\beta_1$  receptor. The recognition of the immobilized receptor was significantly increased for a surface that presented both the primary recognition site (GRGDSP) and the synergy site (PHSRN) compared to the adhesion measured with surfaces that displayed only the GRGDSP peptide. At the collective level, the separation process of the receptor-ligand pairs is a combination of multiple unbinding and stretching events that can accurately be described by the wormlike chain (WLC) model of polymer elasticity. In contrast, stretching was not observed at the single-molecule level. The dissociation of single  $\alpha_5\beta_1$ -GRGDSP pairs under loading rates of 1–305 nN/s revealed the presence of two activation energy barriers in the unbinding process. The high-strength regime above 59 nN/s maps the inner barrier at a distance of 0.09 nm along the direction of the force. Below 59 nN/s a low-strength regime appears with an outer barrier at 2.77 nm and a much slower transition rate that defines the dissociation rate (off-rate) in the absence of force ( $k_{\text{off}}^0 = 0.015 \text{ s}^{-1}$ ).

## Introduction

The ability of cells to bind various membrane and extracellular matrix (ECM) proteins through integrins expressed on cell membranes provides signals that affect the morphology, motility, and survival of cells.<sup>1,2</sup> Better understanding of the molecular mechanisms of integrin-ligand interaction could therefore illuminate several important cell functions. Integrins are membrane glycoproteins with two noncovalently associated subunits, designated  $\alpha$  and  $\beta$ . The combination of  $\alpha$  and  $\beta$  subunits determines the specificity for extracellular ligands as well as intracellular signaling events.<sup>3,4</sup> Although it is unknown how these subunits associate, it is thought that they exist in different conformations according to their activation status: either inactive, where they are unable to bind ligand, or active, where they are capable of binding their ligand.<sup>3</sup> In addition, a cell responds to its environment in part through its ability to regulate the function of integrins by modulating their activity. Both divalent cations and monoclonal antibodies have been used as stimuli to investigate the dynamic regulation of integrin-ligand binding.<sup>3</sup>

In general, ligand binding occurs through recognition by the integrin of a short amino acid sequence from the ligand.<sup>5</sup> The prototype for these integrin binding sites is the Arg-Gly-Asp (RGD) sequence that is present in fibronectin, fibrinogen, vitronectin, and other adhesive

proteins.<sup>5,6</sup> Short peptides containing the RGD sequence can mimic the cell adhesion domains of proteins in two ways: when they are coated on a surface they promote cell adhesion, whereas in solution they can saturate the capacity of the receptor to bind cell adhesion ligands.

This study presents a way to design a biologically active membranelike surface in which ligand accessibility and template composition is used as a means to control the interaction with immobilized  $\alpha_5\beta_1$  integrins. Bioartificial membranes, supported on solid substrates, displaying peptides that mimic the cell binding domain of the ECM protein, fibronectin, are constructed from mixtures of peptide-amphiphiles and poly(ethylene glycol) (PEG) amphiphilic molecules. Peptide-amphiphiles feature  $\text{C}_{16}$  dialkyl ester tails, a Glu (glutamic acid) linker, a  $-(\text{CH}_2)_2$ -spacer, and a headgroup that incorporates the bioactive sequence.<sup>7</sup> The molecular architecture can be controlled thus presenting the peptide in a linear or looped conformation. The tail serves to align the peptide strands and provides a hydrophobic surface for self-association and interaction with other hydrophobic surfaces. The two sequences used in this study are found in the ECM protein, fibronectin: the tenth type III module, GRGDSP (the primary recognition site for  $\alpha_5\beta_1$ ), and the ninth type III module, PHSRN (the synergy binding site for  $\alpha_5\beta_1$ ).

A mixture of the peptide amphiphiles and PEG lipid molecules is deposited on a surface by the Langmuir-Blodgett technique. An atomic force microscope (AFM) is used to provide high-resolution images and direct adhesion measurements. First, we analyzed force profiles at the collective level. When multiple integrin-ligand bonds were involved, force-distance interaction curves exhibited a combination of unbinding and stretching events that were

\* Corresponding author. E-mail: tirrell@engineering.ucsb.edu.

<sup>†</sup> University of Minnesota.

<sup>‡</sup> University of California.

(1) Hynes, R. O. *Cell* **1992**, *69*, 11–25.

(2) Ruoslahti, E.; Reed, J. C. *Cell* **1994**, *77*, 477–478.

(3) Fernandez, C.; Clark, K.; Burrows, L.; Schofield, N. R.; Humphries, M. J. *Frontiers BioSci.* **1998**, *3*, 684–700.

(4) Giancotti, F. G.; Ruoslahti, E. *Science* **1999**, *185*, 1028–1032.

(5) Ruoslahti, E. *Annu. Rev. Cell Dev. Biol.* **1996**, *12*, 697–715.

(6) Pierschbacher, M. D.; Ruoslahti, E. *Nature* **1984**, *309*, 30–33.

(7) Berndt, P.; Fields, G. B.; Tirrell, M. *J. Am. Chem. Soc.* **1995**, *117*, 9515–9522.

fitted to four different models of polymer elasticity. We have also monitored the single-molecule interaction of  $\alpha_5\beta_1$ -GRGDSP pairs under a range of loading rates to investigate the presence of multiple transitions in the unbinding pathway. The spontaneous dissociation (off-rate) reaction rate was also calculated for the  $\alpha_5\beta_1$  from the force spectroscopy experiment, as this is a parameter of prime interest for any biological ligand–receptor system, and results are in agreement with solution off-rates reported for  $\alpha_5\beta_1$  integrins.

Our results demonstrate that our biomimetic system can give an insight into the biophysical character of unbinding processes between  $\alpha_5\beta_1$  receptor-GRGDSP ligand pairs and allow us to understand how different environmental conditions and multiple peptides can enhance the performance of functionalized interfaces.

## Methods

**Preparation and Characterization of Bioartificial Membranes.** 1,2-Distearoyl-*sn*-glycero-3-phosphatidylethanolamine (DSPE) and the PEG chains with molecular weight of 120 covalently linked to DSPE (PEG-120) were obtained from Avanti Polar Lipids, Inc. (Alabaster, AL).  $(C_{16})_2$ -Glu- $C_2$ -KAbuGRGDSPAbuK,  $(C_{16})_2$ -Glu- $C_2$ -KAbuGRGDSPAbuK- $C_2$ -Glu- $(C_{16})_2$ ,  $(C_{16})_2$ -Glu- $C_2$ -KAbuGRGESP-AbuK- $C_2$ -Glu- $(C_{16})_2$ , and  $(C_{16})_2$ -Glu- $C_2$ -PHSRN were synthesized as described elsewhere.<sup>7</sup> For simplicity, these peptide-amphiphiles will be referred as GRGDSP, GRGDSP-looped, GRGESP-looped, and PHSRN, respectively, in the rest of the text.

The pure amphiphiles were dissolved at approximately 1 mg/ml in a 99:1 chloroform/methanol solution. The solution was stored at 4 °C and heated to room temperature prior to use. We used the Langmuir–Blodgett (LB) technique to create supported bioactive bilayer membranes. The LB film depositions were done on a KSV 5000 LB system (KSV Instruments, Helsinki, Finland). All the depositions were done at a surface pressure of 41 mN/m, which is well below the collapse pressure of 60 mN/m. The deposition speed for both the up and down strokes was 1 mm/min. The first step in producing a supported bilayer membrane was to make the mica hydrophobic with a layer of DSPE in the upstroke. The second layer with the peptide-amphiphiles was deposited in the down stroke. The resulting supported bilayer membranes were transferred into glass vials under water. Care was taken to avoid exposing the surfaces to air, as they rearrange to form monolayers and trilayers.<sup>8</sup>

AFM characterization of the LB films was done with a Digital Instruments Nanoscope III system equipped with a fluid cell for tapping mode (Digital Instruments, Santa Barbara, CA). Images were obtained in tapping mode under water using standard 100- $\mu$ m V-shaped silicon nitride AFM cantilevers with pyramidal tips (Digital Instruments) as reported elsewhere.<sup>8</sup>

**$\alpha_5\beta_1$  Immobilization.** Purified human  $\alpha_5\beta_1$  integrins were purchased by Chemicon International (Temecula, CA). The integrins were dialyzed overnight at 4 °C against solution A, pH 7.2, containing 20 mM Tris-HCl (Sigma), 0.1% Triton X-100 (Sigma), 1 mM MgCl<sub>2</sub> (Aldrich), 1 mM MnCl<sub>2</sub> (Aldrich), and 0.5 mM CaCl<sub>2</sub> (Aldrich). The integrins were removed from the dialysis membrane, diluted to 5  $\mu$ g/ml in solution A, aliquoted, and stored at –80 °C.

The integrin immobilization was performed in two different ways. First, we adsorbed  $\alpha_5\beta_1$  integrins on a hydrophobized Si surface. The hydrophobized Si surface was prepared as follows: 1  $\times$  1 cm Si substrate (WaferNet, San Jose, CA) was washed in an ultrasonic cleaner first in acetone and then in isopropyl alcohol for 5 min each, dried with pure N<sub>2</sub>, and exposed to an Ar/H<sub>2</sub>O plasma (Harrick) for 45 s at 250–300 mTorr to generate hydroxyl groups on the surface. The surface was then exposed to vapors of decyltrichlorosilane (Aldrich) for 20 min in a vacuum desiccator, washed with copious amounts of ethanol and heptane, and annealed at 100 °C for 10 min.  $\alpha_5\beta_1$  integrins were incubated on that surface for 2 h at 37 °C and washed with 1 mM MnCl<sub>2</sub>. AFM

images of that surface were taken immediately after the surface was prepared.

For the second method, the integrins were immobilized as follows: a 16- $\mu$ m polystyrene sphere (Bangs Laboratories, Fishers, IN) was attached on the apex of a standard 100- $\mu$ m V-shaped silicon nitride AFM cantilever as described elsewhere,<sup>9</sup> washed with ethanol and phosphate-buffered-saline (PBS) (Life Technologies, Rockville, MD), and coated overnight at 37 °C with goat antiserum to mouse IgG Fc (Cappel, Aurora, OH) at a final antibody concentration of 8  $\mu$ g/mL in PBS. The surface was washed with PBS and nonspecific binding sites were blocked in PBS with 1% BSA (Sigma) and 1:500 Tween 20 (Sigma) at 37 °C for 1 h. The surface was washed with PBS and incubated with purified monoclonal mouse antihuman TS2/16 (anti- $\beta_1$ ) antibody (Endogen, Woburn, MA) in PBS (20  $\mu$ g/mL) for 3 h at 37 °C. After washing and blocking for another hour, purified human  $\alpha_5\beta_1$  integrins were added and incubated at 37 °C for 2 h. Surfaces were washed with PBS before use. AFM images of that surface were taken immediately after the surface was prepared. Integrin activity was verified in our lab by an ELISA test.<sup>10</sup> For the single-molecule force spectroscopy experiments,  $\alpha_5\beta_1$  integrins were immobilized directly on the silicon nitride AFM cantilever as described above without nonspecific blocking with BSA and Tween 20 between steps. To achieve a state in which most of the integrins are blocked and only a small number of  $\alpha_5\beta_1$  can interact with the peptide-amphiphiles, after washing with PBS the tips were incubated with 1 or 5 nM of free GRGDSP (Life Technologies, Rockville, MD) in 1 mM MnCl<sub>2</sub> solution at 37 °C for 1 h. Surfaces were finally washed with PBS before use.

**AFM.** The spring constant of the functionalized 16- $\mu$ m polystyrene probe tips was determined using the resonant frequency method.<sup>11</sup> An average value of 0.59 N/m (SD  $\pm$  0.14 N/m) was used in this study after calibrating 10 probe tips. Surface force measurements were performed using a commercial AFM, a Nanoscope III (Digital Instruments, Santa Barbara, CA), with a fluid cell, at a loading rate, defined as the spring constant of the cantilever times the velocity of the piezo, of 1.16–2.34  $\mu$ N/s. For the single-molecule experiments, three different kinds of V-shaped silicon nitride AFM cantilevers were used with nominal spring constants (provided by the manufacturer) of 0.01, 0.03, and 0.06 N/m (Digital Instruments, Santa Barbara, CA and Thermo-microscopes, Sunnyvale, CA). The loading rate was varied, by changing both the spring constant of the cantilever and the velocity of the piezo, from 1 to 305 nN/s.

Data were recorded as the two surfaces, the sample surface and the probe tip, were brought into contact and then were pulled apart. We show the pull-off force or adhesion force, which is defined as the minimum force that must be applied to separate the two surfaces. All experiments were carried out at room temperature. To minimize the drift effects, we warmed the AFM for at least half an hour before an experiment.

## Results and Discussion

Figure 1 shows topography and phase images of  $\alpha_5\beta_1$  integrins adsorbed on a hydrophobic surface. Phase imaging maps the phase of the cantilever oscillation during a scan to detect variations in composition, adhesion, friction, viscoelasticity, and other properties. Thus, phase imaging provides a clearer observation of fine features often not revealed by topography and can also act as a real-time contrast enhancement technique. Phase imaging, however, cannot provide accurate information about the height of the objects. In Figure 1B, the substrate appears gray and the integrins black. The inside edges, however, are not well defined. The “donut”-shape integrins are on average 46 nm long. Electron microscopy images have shown<sup>12</sup> that two  $\alpha_5\beta_1$  integrins can form a 46-nm-

(9) Kokkoli, E.; Zukoski, C. F. *Langmuir* **2001**, *17*, 369–376.

(10) Dillow, A. K.; Ochsenhirt, S. E.; McCarthy, J. B.; Fields, G. B.; Tirrell, M. *Biomaterials* **2001**, *22*, 1493–1505.

(11) Cleveland, J. P.; Manne, S.; Bocek, D.; Hansma, P. K. *Rev. Sci. Instrum.* **1993**, *64*, 403–405.

(12) Nermut, M. V.; Green, N. M.; Eason, P.; Yamada, S. S.; Yamada, K. M. *EMBO J.* **1988**, *7*, 4093–4099.

(8) Hansma, H. G.; Clegg, D. O.; Kokkoli, E.; Oroudjev, E.; Tirrell, M. *Methods Cell Biol.* **2002**, *69*, 163–193.

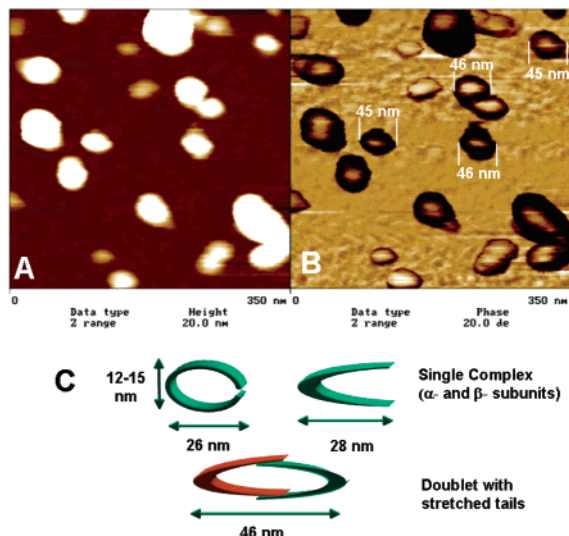


**Figure 1.** AFM images of  $\alpha_5\beta_1$  integrins on a silanized Si surface in tapping mode. (A) Topography image. (B) Phase image. The substrate appears gray and the integrins black. The “donut”-shape integrins are on average 46 nm long. The inside edges, however, are not well defined. Electron microscopy images show that two  $\alpha_5\beta_1$  integrins can form a 46-nm-long doublet (donut-shape object) with overlapping stretched tails.<sup>12</sup> (C) Schematic representation and dimensions of  $\alpha_5\beta_1$  single complexes and doublets with their hydrophobic portions of their tails stretched.<sup>12</sup>

long doublet (donut-shape object) with overlapping stretched tails, as shown in Figure 1C. Phase imaging shows that the adsorbed  $\alpha_5\beta_1$  integrins appear to form doublets rather than single complexes on the silanized Si surface. Force measurements between the adsorbed integrins and GRGDSP surfaces were not reproducible. This observation indicated that the hydrophobic force between the integrin and the silanized Si surface was not strong enough to immobilize them on the probe and as a result the receptor came off the probe and adhered to the other surface. Since the adhesion of the receptor to the hydrophobized substrate should be much stronger than the receptor–ligand binding force, an alternative protocol was pursued.

$\alpha_5\beta_1$  integrins were immobilized on a 16- $\mu\text{m}$  polystyrene sphere with the use of the TS2/16 (anti- $\beta_1$ ) monoclonal antibody. TS2/16 has been shown to enhance cell adhesion by inducing a conformational change at the extracellular domain of the integrin. This high affinity state of the receptor facilitates ligand binding without requiring receptor cross-linking or intracellular signaling pathways.<sup>13</sup> Most importantly, this effect was observed both on intact cells and on detergent-solubilized  $\alpha_5\beta_1$  receptors.<sup>13</sup>

Phase imaging of the immobilized  $\alpha_5\beta_1$  on a polystyrene surface did not show any evidence of doublet formation. Height imaging gave an average of 4.2 nm for the immobilized  $\alpha_5\beta_1$ . This value is in agreement with previous studies that have identified residues 207–218 of  $\beta_1$  subunit as the epitope for stimulatory antibodies such as TS2/16<sup>14</sup> and the structural model for  $\alpha_5\beta_1$  that gives a length of 8 nm for residues 1–446 of the  $\beta_1$  subunit.<sup>12</sup>

**Correction of Force Measurements for Hydrodynamic Drag.** The hydrodynamic drag force was included on all force measurements, with the sphere and the silicon nitride tip. The hydrodynamic drag,  $F_{\text{drag}}$ , is

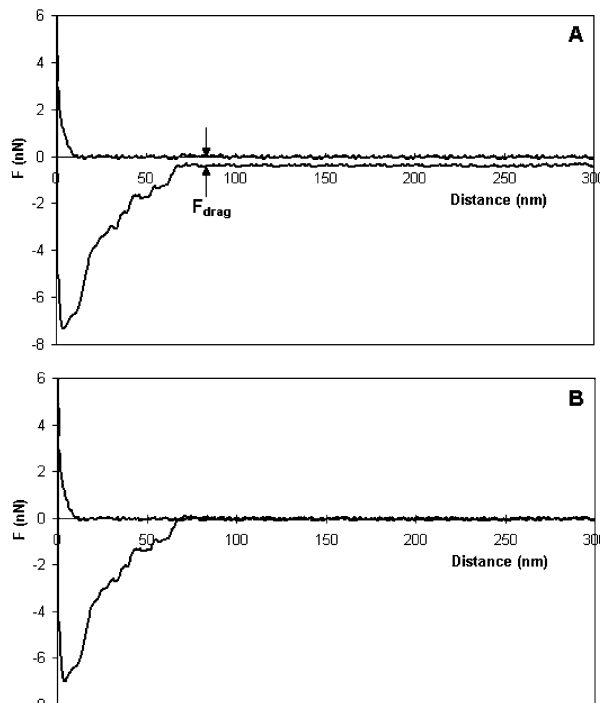


**Figure 2.** (A) Approach (gray color line) and retract (black color line) force–distance curves measured between immobilized  $\alpha_5\beta_1$  integrins on a polystyrene sphere and a peptide-amphiphile bilayer membrane at a piezo velocity of 1.9  $\mu\text{m/s}$  in 0.1 mM  $\text{MnCl}_2$ . The arrows show the hysteresis,  $F_{\text{drag}} = 0.35$  nN, between the approach and retract noncontact lines. (B) Corrected force measurement for hydrodynamic drag. The  $F_{\text{drag}}$ , shown with the arrows in A, has been added to the retracting force profile in A. As a result, the retract force is zero after release, when the two surfaces are not in contact.

the separation of the approach and retract force curve in their noncontact regions,<sup>15,16</sup> as shown in Figure 2A. For each force curve,  $F_{\text{drag}}$  was estimated by measuring the separation of the approach and retract force curve in the noncontact region at small distances and added to the force measured ( $kx$ ) so that  $F = kx + F_{\text{drag}}$ . As a result, retract forces were zero after release, when the surfaces were not in contact (Figure 2B).

For AFM V-shaped silicon nitride cantilevers, the drag coefficient  $\xi$  has been estimated to be 1.55  $\mu\text{Ns/m}$  when the tip and the surface are in contact, and it has been shown that the drag coefficient measured at large tip–surface distances of 2  $\mu\text{m}$  can underestimate the drag factor by 30–50%.<sup>17</sup> Thus, the hydrodynamic drag correction should be measured when the tip and surface are in close proximity. The  $F_{\text{drag}} = \xi U$ , where  $U$  is the relative velocity between the tip and the liquid and can be considered to be approximately equal to the velocity of the piezo. For the single-molecule forces, the  $F_{\text{drag}}$  that was measured experimentally (by measuring the separation of the approach and retract force curve in the noncontact region at small distances) was in good agreement with the one calculated by  $F_{\text{drag}} = \xi U$ , with  $\xi = 1.55$   $\mu\text{Ns/m}$ , for the different piezo velocities applied (35 nm/s–10.5  $\mu\text{m/s}$ ).

The drag coefficient  $\xi$  has been measured experimentally for 10 and 20  $\mu\text{m}$  spheres glued onto AFM cantilevers as a function of the sphere–surface separation.<sup>18</sup> As the

(15) Hoh, J. H.; Engel, A. *Langmuir* **1993**, *9*, 3310–3312.

(16) de Souza, E. F.; Douglas, R. A.; Teschke, O. *Langmuir* **1997**, *13*, 6012–6017.

(17) Alcaraz, J.; Buscemi, L.; Puig-de-Morales, M.; Colchero, J.; Baró, A.; Navajas, D. *Langmuir* **2002**, *18*, 716–721.

(13) Arroyo, A. G.; García-Pardo, A.; Sánchez-Madrid, F. *J. Biol. Chem.* **1993**, *268*, 9863–9868.

(14) Takada, Y.; Puzon, W. *J. Biol. Chem.* **1993**, *268*, 17597–17601.

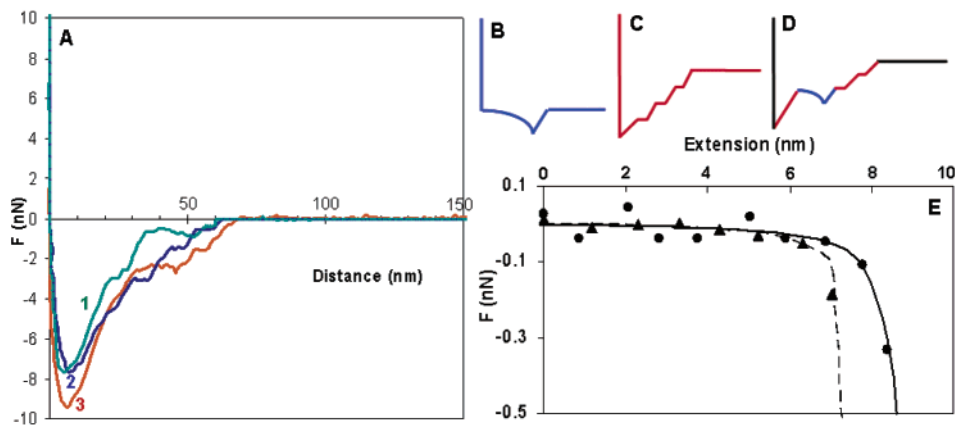


**Figure 3.** (A) Retraction force–distance curves between immobilized  $\alpha_5\beta_1$  integrins on a polystyrene sphere and peptide-amphiphile bilayer membranes in 1 mM  $\text{MnCl}_2$ . (B) A typical chain-extension force curve shows a characteristic negative deflection far from the surface until the chain breaks and then the tip snaps back to its equilibrium position.<sup>19</sup> (C) The unbinding of specific ligand–receptor pairs gives a stepwise profile, as pairs do not break at once but in multiple steps.<sup>20</sup> (D) A combination of the profiles shown in B and C gives this force profile. (E) Normalized force–extension data between  $\alpha_5\beta_1$ -GRGDSP pairs. The  $x$  and  $y$  axis have been shifted so that the onset of the extension has been assigned at zero separation and force. The lines are the WLC fits to the experimental data.

sphere–surface separation decreased, the drag coefficient increased. For very small sphere–surface separations, the normalized drag coefficient is approximately  $\xi/\xi_\infty = 30\text{--}38$ , where  $\xi_\infty$  is the drag coefficient at infinite separation, with  $\xi_\infty \sim 2\text{--}5 \mu\text{Ns/m}$ .<sup>18</sup> Therefore, for a  $10\text{--}20 \mu\text{m}$  colloidal probe tip,  $\xi$  can vary between  $60\text{--}190 \mu\text{Ns/m}$ . For the force curve shown in Figure 2,  $U = 1.9 \mu\text{m/s}$  and accordingly  $F_{\text{drag}} = \xi U = 0.11\text{--}0.36 \text{ nN}$  which is in good agreement with the experimental result  $F_{\text{drag}} = 0.35 \text{ nN}$  (Figure 2A). The experimental hydrodynamic forces that we measured with the polystyrene sphere varied between 0.1 and 0.4 nN.

**Analysis of Collective Ligand–Receptor Unbinding Events.** Retraction AFM force–distance curves, after the two surfaces are in contact, are shown in Figure 3A. The separation of  $\alpha_5\beta_1$ -GRGDSP pairs produces two kinds of force profiles: Curve 2 in Figure 3A is a stepwise profile similar to the one shown in Figure 3C. In this case, the ligand–receptor pairs do not break at once but in multiple steps, thus producing a stepwise return to zero force. Curves 1 and 3 in Figure 3A show a close resemblance to Figure 3D. Figure 3D is a combination of the profiles shown in Figure 3B, a chain-extension force curve, and Figure 3C, a stepwise unbinding of ligand–receptor pairs. Thus, curves 1 and 3 demonstrate a combination of multiple unbinding and stretching events between the  $\alpha_5\beta_1$ -GRGDSP pairs. Simulations of the adhesion bonds between ligand–receptor pairs in a force probe experiment illustrate the simultaneous breaking of bonds at the edge of the contact area and the increased stretching of bonds in the center.<sup>21</sup>

The stretching events could be due to the stretching of ligand–receptor pairs, stretching of polystyrene chains from the sphere, or from denatured IgG molecules that are nonspecifically adsorbed on the sphere. Extension curves have been observed on collective forces measured for  $\alpha_5\beta_1$  integrins immobilized either on polystyrene spheres or on silicon nitride tips (the tips were not blocked

with free GRGDSP thus allowing multiple integrin interactions). Therefore, since stretching events have been observed for multiple  $\alpha_5\beta_1$  pairs immobilized on different substrates, it excludes the possibility that this is an artifact attributed to polystyrene chain pulling. The possibility of a small number of denatured IgGs adsorbed on the polystyrene surface cannot be eliminated. However, their effect on the reported measurements should be insignificant on the basis of the following argument. Denatured IgGs have a decreased capacity for antigen binding.<sup>22,23</sup> As a result, they should not be able to bind the TS2/16 molecules. More likely, they will be covered by neighboring TS2/16- $\alpha_5\beta_1$  molecular chains thus preventing them from contributing to the observed traces. The height of the TS2/16- $\alpha_5\beta_1$  molecular chains is estimated to be 13 nm (approximately 8.5 nm the height of the antibody<sup>24</sup> and 4.2 of the  $\alpha_5\beta_1$  as indicated by our AFM measurements) and our AFM images do not show the presence of 13-nm steps thus excluding the possibility that denatured IgGs are exposed at the interface. We therefore suggest that the extension contours come from the stretching of  $\alpha_5\beta_1$ -GRGDSP pairs. Integrin stretching has been implicated before between RGD peptides covalently coupled to AFM tips and platelet  $\alpha_{\text{IIb}}\beta_3$  integrins from interactions between the functionalized AFM tips and platelets deposited on glass substrates.<sup>25</sup> The authors observed a delay in debonding force that was interpreted as stretching of the bonded  $\alpha_{\text{IIb}}\beta_3$  receptors (the authors did not fit their data to any models of polymer elasticity).

Force-normalized extension data are shown in Figure 3E. The  $x$  and  $y$  axis have been shifted so that the onset of the force extension has been assigned at zero separation and force. Four different models of polymer elasticity were used to fit the data, the wormlike chain (WLC),<sup>26</sup> the freely joined chain (FJC),<sup>27</sup> the modified WLC,<sup>28</sup> and the modified

(18) Benmouna, F.; Johannsmann, D. *Eur. Phys. J. E* **2002**, *9*, 435–441.

(19) Butt, H.-J.; Kappl, M.; Mueller, H.; Raiteri, R.; Meyer, W.; Rühle, J. *Langmuir* **1999**, *15*, 2559–2565.

(20) Florin, E.-L.; Moy, V. T.; Gaub, H. E. *Science* **1994**, *264*, 415–417.

(21) Vijayendran, R.; Hammer, D.; Leckband, D. *J. Chem. Phys.* **1998**, *108*, 7783–7794.

(22) Vermeer, A. W. P.; Bremer, M. G. E. G.; Norde, W. *Biochim. Biophys. Acta* **1998**, *1425*, 1–12.

(23) Vermeer, A. W. P.; Norde, W.; van Amerongen, A. *Biophys. J.* **2000**, *79*, 2150–2154.

(24) Silverton, E. W.; Navia, M. A.; Davies, M. A. *PNAS* **1977**, *74*, 5140–5144.

(25) Lee, I.; Marchant, R. E. *Surf. Sci.* **2001**, *491*, 433–443.

(26) Bustamante, C.; Marko, J. F.; Siggia, E. D.; Smith S. *Science* **1994**, *265*, 1599–1600.

(27) Butt, H.-J.; Kappl, M.; Mueller, H.; Raiteri, R. *Langmuir* **1999**, *15*, 2559–2565.

(28) Odijk, T. *Macromolecules* **1995**, *28*, 7016–7018.

FJC model<sup>29</sup> (supporting text has all the equations and Figure 10 shows all fits to the data, which are published as Supporting Information on the Langmuir Web site). The best fit to the data was given by the WLC model (Figure 3E):

$$F(x) = \left(\frac{k_B T}{l}\right) \left[ \frac{1}{4} \left(1 - \frac{x}{L_c}\right)^{-2} - \frac{1}{4} + \frac{x}{L_c} \right] \quad (1)$$

where  $k_B$  is the Boltzmann constant,  $T$  is the temperature,  $l$  is the persistence length (the length of the statistical segment), and  $L_c$  is the contour length, which is equal to  $nl$ , where  $n$  is the total number of statistical segments. A value of 0.37 nm was used for  $l$ , which is the contour length of a peptide residue.<sup>30</sup> If the persistence length is also allowed to vary in the fitting, then  $l = 0.37 \pm 0.02$  nm. From the fit to the data,  $L_c = 8 \pm 1.3$  nm. That length corresponds to the stretching of  $n = 22 \pm 4$  amino acids of the  $\alpha_5\beta_1$ -GRGDSP pairs. The elasticity of the system, which corresponds to the slope of the force extension curve just before rupture, was  $0.25 \pm 0.12$  nN/nm. The elasticity of the system is a measure of its extensibility and can be thought of as the spring constant of the system. A direct correlation between the elasticity of the system and the molecular spring constant of a single receptor–ligand pair is difficult to obtain since the number of bonds involved is unknown.

#### Specificity, Effect of PEG, and the Ssynergy Site.

For the analysis of these data, only the last step of the unbinding force curves was considered, as the other steps are a nonlinear convolution of multiple unbinding and stretching events between the  $\alpha_5\beta_1$  functionalized sphere and the bioartificial membrane. Therefore, during the analysis only the unbinding of a small number of pairs was considered. This number can vary from one measurement to another and error bars have been included in our graphs to show the standard deviation from the average values that we report.

Specificity was confirmed in two ways, by varying the ion concentration and by using an inactive peptide-amphiphile for negative control. The role of divalent cations in integrin function is demonstrated in the literature by the lack of ligand binding upon removal of cations by chelating agents.<sup>3</sup> Furthermore, divalent cations such as  $Mn^{2+}$ ,  $Mg^{2+}$ , and  $Ca^{2+}$  have distinct effects on integrin function in vitro. Generally,  $Mn^{2+}$  confers high affinity binding properties on isolated integrins, whereas  $Ca^{2+}$  inhibits ligand binding, with  $Mg^{2+}$  playing a stimulatory role but to a lesser extent than  $Mn^{2+}$ .<sup>3</sup> Earlier studies on the  $\alpha_5\beta_1$  receptor have demonstrated the presence of at least three distinct classes of cation binding sites for  $Mn^{2+}$ ,  $Mg^{2+}$ , and  $Ca^{2+}$ .<sup>31</sup> Ligand binding supported by  $Mn^{2+}$  was inhibited by  $Ca^{2+}$  in a noncompetitive manner implying distinct binding sites for these two cations and a second site that can bind  $Mg^{2+}$  or  $Ca^{2+}$  in a competitive manner was also observed. The effect of  $Mn^{2+}$  and  $Ca^{2+}$  ions on the immobilized  $\alpha_5\beta_1$  integrins is shown in Figure 4.  $Mn^{2+}$  ions increase the adhesion of the immobilized  $\alpha_5\beta_1$  to the GRGDSP ligands, whereas  $Ca^{2+}$  ions decrease it. Loss of integrin activity is shown by addition of EDTA that chelates cations. Specificity was also established by using inactive peptides such as GRGESP as a negative control experiment. Figure 5 shows that the  $\alpha_5\beta_1$  integrins

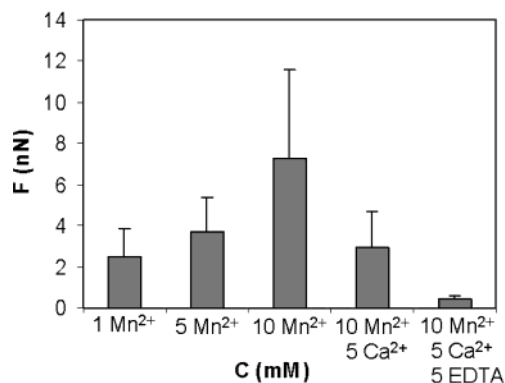


**Figure 4.** Effect of divalent cations on the specific binding of  $\alpha_5\beta_1$ -GRGDSP. The same sphere was used for these measurements. Data correspond to the average value that resulted from 20 to 25 force measurements all over the surface. The error bars represent the standard deviation and reflect the fact that the number of pairs that interact can vary from one measurement to another.  $Mn^{2+}$  ions increase the binding affinity of  $\alpha_5\beta_1$  for GRGDSP, and  $Ca^{2+}$  ions inhibit it. Loss of integrin activity is shown upon removal of cations by EDTA, a chelating agent.

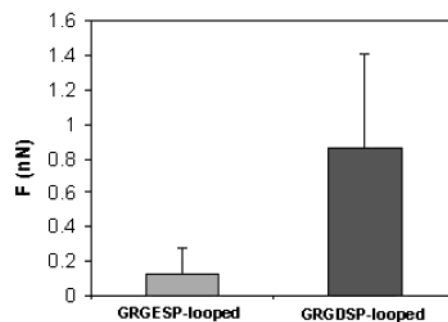


**Figure 5.** Specificity of  $\alpha_5\beta_1$  in the presence of 1 mM  $MnCl_2$ . The  $\alpha_5\beta_1$  integrins bind preferentially to the GRGDSP-looped surface and not to the GRGESP-looped surface. The same sphere was used for both measurements. The data shown are average values from 25 to 30 measurements on each surface. The error bars represent the standard deviation and reflect the fact that the number of pairs that interact vary from one measurement to another.

bind preferentially to the GRGDSP-looped peptide but not to the GRGESP-looped surface.

Poly(ethylene glycol) molecules are used extensively in biomaterials research since they prevent protein adsorption. In contrast to the peptide-amphiphiles, PEG lipids are effective in preventing protein and cell adhesion to surfaces.<sup>32,33</sup> In this study, the effect of short PEG molecules, relative to the peptide-amphiphile height, has been examined. Figure 6 shows that the receptors do not adhere to a surface fully covered with PEG-120. In contrast, the immobilized  $\alpha_5\beta_1$  receptors adhere to the mixed PEG-120 membranes (50% GRGDSP–50% PEG-120) and the pure GRGDSP bilayer. Similar results have been shown with cell studies where cells adhere and spread on 50% mixtures of peptide-amphiphiles with PEG lipids having chains of 120 molecular weight.<sup>32</sup>

The RGD motif in fibronectin is the critical recognition site for  $\alpha_5\beta_1$ , but the synergy site PHSRN is also required for high affinity binding.<sup>34</sup> This high affinity binding was tested with bioartificial membranes that had

(29) Smith, S. B.; Finzi, L.; Bustamante, C. *Science* **1992**, *258*, 1122–1126.

(30) Idiris, A.; Alam, M. T.; Ikai, A. *Protein Eng.* **2000**, *13*, 763–770.

(31) Mould, A. P.; Akiyama, S. K.; Humphries, M. J. *J. Biol. Chem.* **1995**, *270*, 26270–26277.

(32) Dori, Y.; Bianco-Peled, H.; Satija, S. K.; Fields, G. B.; McCarthy, J. B.; Tirrell, M. *J. Biomed. Mater. Res.* **2000**, *50*, 75–81.

(33) Sigal, G. B.; Mrksich, M.; Whitesides, G. M. *J. Am. Chem. Soc.* **1998**, *120*, 3564–3473.

(34) Aota, S.; Nomizu, M.; Yamada, K. M. *J. Biol. Chem.* **1994**, *269*, 24756–24761.

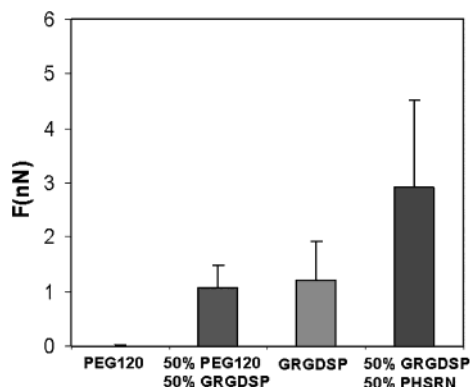


**Figure 6.** Effect of PEG-120 and PHSRN in the presence of 1 mM  $\text{MnCl}_2$ . Each column corresponds to a different sphere and is the average of 25–30 measurements on each surface. Data correspond to the average values. The error bars show standard deviations and reflect the fact that the number of pairs that interact can vary from one measurement to another. Because different spheres were used, direct comparisons are difficult to make; however, qualitative comparisons remain valid.  $\alpha_5\beta_1$  integrins do not bind to the PEG-120 surface. 50% GRGDSP with 50% PEG-120 has similar effect as a 100% GRGDSP surface on the specific recognition of  $\alpha_5\beta_1$ . The binding affinity of the receptor is significantly increased for a surface that has 50% GRGDSP–50% PHSRN peptide amphiphiles.

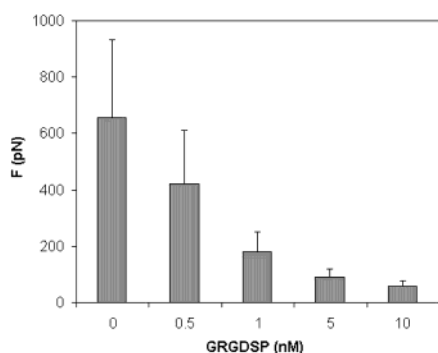


**Figure 7.** Effect of soluble GRGDSP on the specific binding of  $\alpha_5\beta_1$ -GRGDSP. Forces were measured at a loading rate of 59 nN/s in 1 mM  $\text{MnCl}_2$ . Different tips were used for these measurements with nominal radii (provided by the manufacturer) that varied 5–40 nm. Each column corresponds to a different tip and is the average of 65 force measurements all over the surface. The error bars represent the standard deviation and reflect the fact that the number of pairs that interact can vary from one measurement to another.

50% GRGDSP–50% PHSRN peptide-amphiphiles. Indeed, the specific recognition of the immobilized receptor was significantly increased for a surface that presented both the primary recognition site (GRGDSP) and the synergy site (PHSRN) compared to the adhesion measured with surfaces that had 50% GRGDSP–50% PEG-120 or 100% GRGDSP.

**Force Spectroscopy.** For the single-molecule force spectroscopy experiments, pure  $\alpha_5\beta_1$  integrins were immobilized on the silicon nitride AFM tip and blocked with free GRGDSP as described in the methods section. The effect of the GRGDSP concentration on the  $\alpha_5\beta_1$  adhesion blocking is shown in Figure 7. For the single-molecule force measurements, tips with different radii were used and incubated with 1 or 5 nM of free GRGDSP.

Stretching events were not observed at the single-molecule level only at the collective level. Structural deformations of multiple molecules at the nanoscale can give rise to a broad range of configurations and thus to very different conditions of loading for multiple bonds

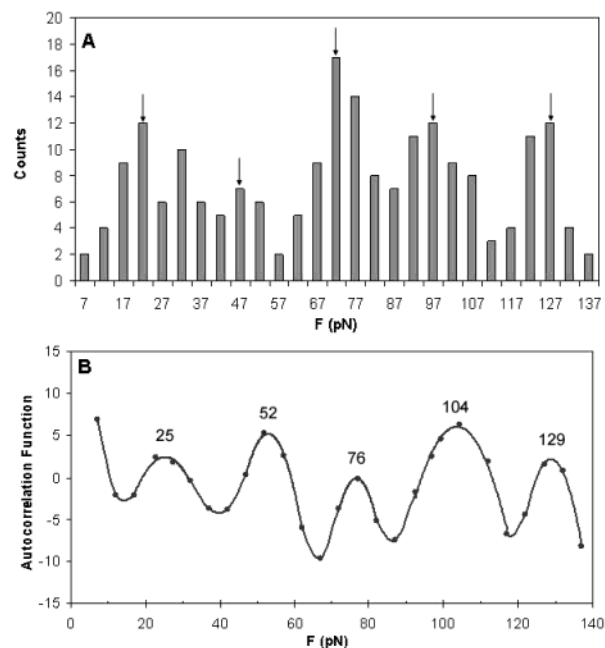


**Figure 8.** (A) Histogram of unbinding forces between  $\alpha_5\beta_1$ -GRGDSP pairs in 1 mM  $\text{MnCl}_2$ . The graph shows 245 out of 750 individual force curves (the rest are zero) that were collected at a loading rate of 59 nN/s. Arrows point to peaks with a periodicity of  $22 \pm 3$  pN. (B) Autocorrelation function for the histogram of forces shown in Figure 8A. The periodicity is 25 pN.

versus loading for single-molecule bonds.<sup>35</sup> Our data demonstrate that integrins may behave in a different manner when they interact collectively versus when they interact individually.

Force histograms were collected at loading rates of 1–305 nN/s. The bond strength at a specific loading rate was estimated either by inspection of the force histogram or by calculating the autocorrelation function for that histogram.<sup>36</sup> The autocorrelation function reveals weak periodic signals in noisy data. It was used as a tool to filter the noise from the data and clearly shows the periodicity of the force measurements. Both methods gave similar results. An example is shown in Figure 8 for a loading rate of 59 nN/s. The histogram of forces in Figure 8A gives a bond strength of  $22 \pm 3$  pN. The autocorrelation function in Figure 8B shows five peaks that are all multiples of 25 pN. Thus, the pronounced periodicity of the autocorrelation function in Figure 8B reveals that the unbinding forces in Figure 8A are composed of integer multiples of an elementary force quantum of 25 pN. Previous studies have reported the  $\alpha_5\beta_1$ -GRGDSP bond strength to be  $32 \pm 2$  pN (the authors serially reduced the retraction rate from 50 to 1  $\mu\text{m/s}$  until individual unbinding events were detected) for AFM measurements between osteoblast cells and GRGDSP ligands<sup>37</sup> and in the order of 13–28 pN at a loading rate of 5–100 pN/s for optical tweezers experiments between fibroblasts and fibronectin.<sup>38</sup>

The possibility of membrane failure via extraction of peptide-amphiphiles was investigated by comparing our

(35) Evans, E. *Annu. Rev. Biophys. Biomol. Struct.* **2001**, *30*, 105–128.

(36) Schönherr, H.; Beulen, M. W. J.; Bügler, J.; Huskens, J.; van Veggel, F. C. J. M.; Reinhoudt, D. N.; Vancso, G. J. *J. Am. Chem. Soc.* **2000**, *122*, 4963–4967.

(37) Lehenkari, P. P.; Horton, M. A. *Biochem. Biophys. Res. Commun.* **1999**, *259*, 645–650.

(38) Thoumine, O.; Kocian, P.; Kottelat, A.; Meister, J.-J. *Eur. Biophys. J.* **2000**, *29*, 398–408.

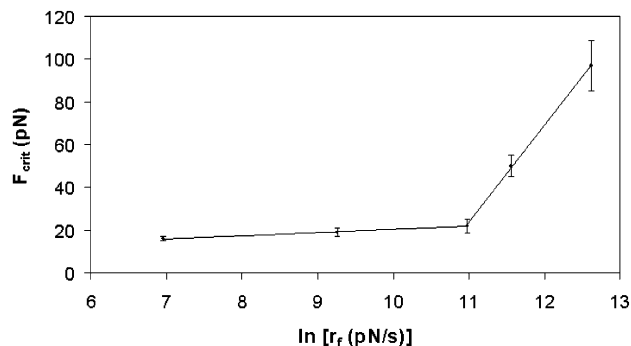


**Figure 9.** Rupture force for  $\alpha_5\beta_1$ -GRGDSP bond versus the logarithm of loading rate (pN/s). The error bars represent the standard deviations in each force histogram. A total of 4000 individual forces have been analyzed for this graph. The lines are the Bell model fits.

data to the forces measured for the extraction of lipids from lipid bilayers.<sup>39</sup> For comparable rates of 1–10 nN/s, the force required to extract a lipid is 30–44 pN<sup>39</sup> whereas the unbinding force of a single  $\alpha_5\beta_1$ -GRGDSP pair is 16–19 pN. Therefore, under these conditions lipid anchoring is stronger and the integrin bond will unbind first.

The unbinding force versus the logarithm of the loading rate for single  $\alpha_5\beta_1$ -GRGDSP bonds is plotted in Figure 9. The force spectrum revealed two linear regimes with different slopes, within the range of loading rates that were examined. Thus, the  $\alpha_5\beta_1$ -GRGDSP complex overcomes two transitions during its dissociation under applied force. It is important to know what is the sensitivity of the  $\alpha_5\beta_1$ -GRGDSP bond dissociation under these two transitions. The Bell parameters ( $x_B$  and  $k_{off}^\circ$ ) can provide a measure of that. The  $x_B$  has dimensions of length and describes the separation difference between the bound and the unbound state for the transition state. It may be considered to be the bond interaction length and a measure of the sensitivity of the ligand–receptor adhesion to the applied force.<sup>40</sup> The  $k_{off}^\circ$  ( $k_{off}^\circ = 1/t_{off}$ , where  $t_{off}$  is the bond lifetime) is the dissociation rate (off-rate) in the absence of applied force. Both  $k_{off}^\circ$  and  $x_B$  are important parameters in determining the susceptibility of the bond dissociation to applied force or under flow conditions.<sup>41</sup> Furthermore, these two kinetic parameters are more important than the affinity of the receptor for the ligand in determining both the magnitude and extend of cell adhesion.<sup>40</sup>

The Bell parameters ( $x_B$  and  $k_{off}^\circ$ ) can be estimated from the slope and the intercept of force versus the logarithm of the loading rate:<sup>42,43</sup>

$$F = \frac{k_B T}{x_B} \ln\left(\frac{x_B}{k_{off}^\circ k_B T}\right) + \frac{k_B T}{x_B} \ln r_f \quad (2)$$

where  $F$  is the unbinding force per bond,  $k_B$  is the Boltzmann constant,  $T$  is the absolute temperature,  $x_B$  describes the separation difference between the bound and the transition state projected along the direction of the force,  $k_{off}^\circ$  is the dissociation rate in the absence of applied force, and  $r_f$  is the loading rate. The best fits to the data reveal an inner barrier for loading rates above

59 nN/s at  $x_B = 0.09$  nm that is characterized by a very rapid unstressed transition rate of  $1/t_{off} = 787$  per sec. Below 59 nN/s, a second regime appears in the force spectrum that maps an outer barrier at  $x_B = 2.77$  nm. The outer barrier is characterized by a much slower transition rate that defines the off-rate in the absence of force,  $k_{off}^\circ = 0.015$  s<sup>-1</sup>. This value is in good agreement with the dissociation rate constant of 0.01 s<sup>-1</sup> reported between fibronectin and the fibronectin receptor ( $\alpha_5\beta_1$ ) on fibroblast cells in solution.<sup>44</sup> A  $k_{off}^\circ = 0.012$  s<sup>-1</sup> was recently reported from single-molecule AFM measurements between K562 cells, that express the  $\alpha_5\beta_1$  integrins, and human plasma fibronectin.<sup>45</sup> The  $k_{off}^\circ = 0.015$  s<sup>-1</sup> reported here from a purely biomimetic cell-free system that consists of immobilized  $\alpha_5\beta_1$  receptors and GRGDSP ligands is in excellent agreement with the recently reported value of 0.012 s<sup>-1</sup> measured from cell–protein interactions.

## Conclusions

We have engineered a novel biomimetic system that allows us to study the mechanistic details of the unbinding processes of  $\alpha_5\beta_1$ -GRGDSP pairs at the collective and single-molecule level, and we use this complex to understand how different conditions and multiple peptides can enhance the adhesion of  $\alpha_5\beta_1$ . For example, stronger adhesion can be achieved if the surface is functionalized with peptides that mimic both the main recognition site (GRGDSP) for integrins and the synergy site (PHSRN) of the cell adhesion domain of fibronectin. We have worked with pure integrins to focus on receptor–ligand interactions as purely as possible without complicated features associated with real cells, such as membrane diffusion, cell viscoelastic deformation behavior, and receptor/cytoskeletal interactions.<sup>46</sup> Because of the simplified nature of this system, important insights can be gained into the biophysical character of the unbinding interaction between ligand–receptor pairs.

We demonstrate for the first time that at the collective level the separation of multiple identical bonds, that of the  $\alpha_5\beta_1$ -GRGDSP, is a combination of multiple unbinding events, as the pairs do not break at once but in multiple steps, and stretching processes. The best fit to the force-extension data was given by the WLC model with a contour length of  $8 \pm 1.3$  nm that corresponds to the stretching of  $22 \pm 4$  amino acids of the  $\alpha_5\beta_1$ -GRGDSP pair. Stretching has not been observed at the single-molecule level. At the collective level, however, there are multiple bonds and as force is applied to break a population of pairs it is possible to observe stretching of some bonds. Our data demonstrate that integrins may behave in a different manner when they interact collectively versus when they interact individually.

The specificity of the  $\alpha_5\beta_1$  integrin for the GRGDSP ligand was established by varying the concentration of divalent cations, by using chelating agents, and by using an inactive peptide-amphiphile (GRGESP) as a negative control experiment. It was shown that  $Mn^{2+}$  and  $Ca^{2+}$  had a distinct effect on the immobilized integrins. As in the integrins that are part of a cell membrane,  $Mn^{2+}$  increased the adhesion of the immobilized  $\alpha_5\beta_1$  for the GRGDSP peptide-amphiphile,  $Ca^{2+}$  decreased it, and loss of integrin activity was shown by adding the chelating agent EDTA.

(39) Evans, E.; Ludwig, F. *J. Phys.: Condens. Matter* **2000**, *12*, A315–A320.

(40) Orsello, C. E.; Lauffenburger, D. A.; Hammer, D. A. *Trends Biotechnol.* **2001**, *19*, 310–316.

(41) Alon, R.; Chen, S. Q.; Puri, K. D.; Finger, E. B.; Springer, T. A. *J. Cell Biol.* **1997**, *138*, 1169–1180.

(42) Evans, E.; Ritchie, K. *Biophys. J.* **1997**, *72*, 1541–1555.

(43) Tees, D. F. J.; Waugh, R. E.; Hammer, D. A. *Biophys. J.* **2001**, *80*, 668–682.

(44) Lauffenburger, D. A.; Linderman, J. J. *Receptors: Models for Binding, Trafficking, and Signaling*; Oxford University Press: New York, 1993.

(45) Li, F.; Redick, S. D.; Erickson, H. P.; Moy, V. T. *Biophys. J.* **2003**, *84*, 1252–1262.

(46) Kuo, S. C.; Lauffenburger, D. A. *Biophys. J.* **1993**, *65*, 2191–2200.

The strength of the  $\alpha_5\beta_1$ -GRGDSP single bond varied between 15 and 109 pN for loading rates 1–305 nN/s. The adhesion measured after surface separation cannot be attributed to membrane failure as the force required to pull lipids from the bilayer is significantly higher than the forces measured with this system for comparable loading rates. Under these conditions, lipid anchoring is stronger and the integrin bond will unbind first. Dynamic force spectroscopy revealed that the  $\alpha_5\beta_1$ -GRGDSP dissociation is characterized by two barriers. The outer barrier at a distance of 2.77 nm is governing the rate of spontaneous dissociation in solution while the inner one at 0.09 nm becomes rate-limiting in the presence of much higher loading rates. The off-rate was  $0.015\text{ s}^{-1}$ , which is in agreement with solution and AFM cell measurements for  $\alpha_5\beta_1$  integrins. Thus, our experiments show that our biomimetic system can accurately predict the solution off-

rate parameter, one of the main determinants of the affinity of the integrin–ligand system.

**Acknowledgment.** We thank Dr. Angela K. Dillow for helpful discussions. This work was partially supported by the MRSEC Program of the National Science Foundation under Award No. DMR00-80034 at the University of California in Santa Barbara and partially by National Institutes of Health Grant HL 62427-01. Support from the University of Minnesota MRSEC Artificial Tissues Program (DMR99-09364) is also acknowledged with appreciation.

**Supporting Information Available:** Equations used and all fits to the data. This material is available free of charge via the Internet at <http://pubs.acs.org>.

LA035597L